Full Length Research Article

STRUCTURAL AND OPTICAL STUDIES OF ZNO NANORODS PREPARED OF NANORODS PREPARED BY HYDROTHERMAL METHOD

*Ayyasamy, A. and Dr. Thanapathi, G.

Poomopuhar College, Nagapattinam, Tamilnadu, India

ARTICLE INFO	ABSTRACT

Zinc oxide (ZnO), a representative of II–VI semiconductor compounds, is a very versatile and important material. ZnO has a unique position among semiconducting oxides due to its piezoelectric and transparent conducting properties. It has a high electrical conductivity and optical transmittance in the visible region. Zinc oxide (ZnO) has extensive commercial use during the past 100 years. It has useful optical, chemical and electrical properties, and is nontoxic, inexpensive and chemically stable. ZnO, a semiconductor with a direct wide band gap of 3.37 eV at room temperature and large exciton binding energy of 60 meV, is one of the most promising materials for the fabrication of optoelectronic devices operating in the blue and ultraviolet (UV) regions and gas sensing applications (Djurisic *et al*., 2010 and Michelle, 2012). It has a wide range of technological applications including transparent conducting electrodes of solar cells, flat panel displays, surface acoustic devices, chemical and biological sensors and UV lasers (Zhong Lin Wang, 2004; http://www.chemistry.ohio-state.edu/~woodward/ch754/struct/ZnO.htm; Zhiyong Fan and Jia G. Lu, 2005; Baruah and J Dutta, 2009). Controlled synthesis of semiconductor nanostructures in terms of size and shape has strong motivation to researchers because their properties can be controlled by shape and size. Novel applications can be investigated and are dependent of their structural properties. As the morphology of nano-materials is one of the key factors that affect their properties. ZnO nano-structures with novel morphologies are therefore needed urgently. To date, ZnO with different nanostructures, such as nanotetrapods, combs-like, nanoneedles, nano-flowers, nanorods, nanowires, nanobelts, nanotubes, nanorings and nanosheets (Baruah and J Dutta, 2009; Ahsanulhaq Qurashi, 2013; Xiaobin Xu, 2012; Juan Xie *et al*., 2009; Fanfei Bai *et al*., 2005; Xudong Wang, 2007, Zhong Lin Wang, 2014 and Wang *et al*., 2011), have been successfully synthesized. During the past few years, attention has been focused on the research field of one-dimensional (1D) nanostructure materials, such as nanowires and nanorods, because of their fundamental importance and the wide range of potential applications for nanodevices (Djurisic, 2010). One-dimensional (1D) ZnO have been prepared by various methods such as thermal evaporation, cyclic feeding chemical vapor deposition, chemical vapor deposition (CVD), metal–organic CVD, vapor–liquid–solid (VLS), metal organic chemical vapor deposition (MOCVD), arc discharge and laser ablation (Chen *et al*., 2004; Sekar *et al*., 2005; Zhang, 2005 and Subramanyam, 2000). However, these methods involve special equipment, complex process controlling or high temperature as unfavorable for industrialization. As a result; it is conceived that the preparation of 1D ZnO nano/micro structures via wet chemical routes such as template-based method, hydrothermal process, solvothermal process, microwave-heating route, ultrasonic technique (Tian *et al*., 2011; Law *et al*., 2005; Saito and Haneda, 2011 and Ghule, 2011) can produce such structures, with better crystal quality preferably at lower growth temperature. It works out to be an easier and economical process as well. For the present research, ZnO nanocrystals were synthesized using microwave and ultrasonic radiations. A number of reaction conditions for example solvents, surfactants, precursors, acidity and basicity were used to synthesize ZnO nanocrystal with difference morphologies. The effects of the reaction conditions on the final products were systematically investigated.

INTRODUCTION

Characterization Techniques

The intension of this chapter is to elucidate the basic principles and instrumentation of various techniques used in this report. Structural characterization was done using powder X-ray diffraction (XRD). Particle surface morphology was carried out using Scanning Electron Microscopy (SEM).

Corresponding author: Ayyasamy, A.,
Poomopuhar College, Nagapattinam, Tamilnadu, India.

The elementary analysis was done by Energy Dispersive X-ray spectroscopy (EDX). Optical properties were determined by UV-Visible and photoluminescence spectroscopy.

Powder X-ray diffraction (XRD)

X-ray powder diffraction is a non-destructive technique widely applied for phase identification, crystal structure determination, compositional, the determination of micro structural properties (crystallinity, crystallite size, grain orientation etc), stress and strain. In this study, the

diffractometer supplied by RICH SEIFERT, Germany (model 3000) was used. The $K\alpha_1$ (λ=1.5406 Å) radiation from a copper target was selected using a curved quartz crystal as primary monochromater for line focus. A NaI (Tl) scintillator was used as the detector and the detector could be moved over the diffraction space under computer control. The diffractometer optimized to θ-θ geometry. The detector resolution was upto 0.001^0 in θ. The powder specimen spread on a mylar foil was mounted on a sample holder and presented in the transmission mode. The angles and intensities of diffractions are recorded electronically using a detector, electronics and specialized software resulting in a plot of 2θ (horizontal axis) vs. intensity (vertical axis) for the specimen.

Bragg's law

In 1912 W.L. Bragg proposed a simple way of understanding of X-ray diffraction by crystalline materials. The crystal lattice is a three dimensional array of atoms in space with the lattice planes separated by a distance d. When a monochromatic X-rays fall on the crystalline surface they are scattered and gives rise to interference phenomenon. The diffracted X-rays from various planes with integral multiple (n) of wavelength (λ) will interfere constructively and results in a large output signal at the corresponding angles in the spectrum. The diffraction with half integral multiple of wavelength will interfere destructively and will cancel each other's effect.

According to Figure 2.1, there is a path difference between rays reflected from plane 1 and adjacent plane 2 in the crystal. The two reflected rays will reinforce each other, only when this path difference is equal to an integral multiple of the wavelength. If d is the interplanar spacing, the path difference is twice the distance $d_{hkl}\sin\theta$. The Bragg condition for reflection can be written as:

$$2d_{hkl}\sin\theta = n\lambda \quad\quad\quad \text{.........................(1)}$$

Where, n (an integer) is the order of reflection

λ is the wavelength of the incident rays
d is the interplanar spacing
θ is the angle of incidence.

Structure determination

Phase identification is accomplished by comparing the data (peaks and relative intensities) obtained for our specimen with peaks and relative intensities from a very large set of "standard" data provided *by Joint Committee on Powder Diffraction Standards (JCPDS)*. From that data, we can identify as well confirm the structure of unknown materials.

Grain size determination

The X-ray diffracted line broadening can be used to determine the mean crystallite size (D) using Scherrer formula as follows:

$$D = \frac{K\lambda}{\beta\cos\theta} \quad\quad\quad \text{..............................(2)}$$

Where, K is the shape factor

λ is wavelength of incident X-rays (1.5406 Å)

β is full-width at half maximum of the peaks
θ is diffraction angle.

Scanning electron microscopy (SEM)

Scanning Electron Microscopes are scientific instruments that use a beam of highly energetic electrons to examine objects on a very fine scale. This examination can yield information about the topography (surface features of an object) and surface morphology (shape and size of the particles making up the object). SEM has higher depth of field, higher resolution and larger magnification. The beam of electrons is produced by an electron source that can be made of many different materials depend upon the nature of the source (like thermo-ionic or field emission source). The beam of electrons is attracted by the anode, which is put at higher positive potential. In the case of thermionic source there is a cloud of electrons in the vacuum because the electrons are given high energy to overcome the work function of material and then accelerated by the anode, while for field emission (FE) source the electrons are extracted from the material through a high electric field and the tunneled electrons are then accelerated by the anode.
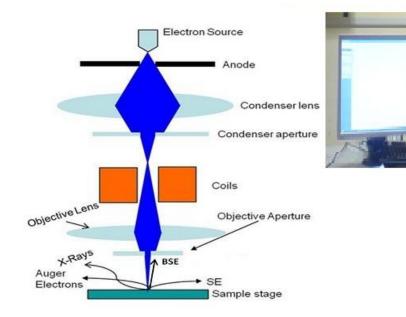

Figure 2.2. Schematic of scanning electron microscope (SEM)

This beam is then passed through a condenser lens to demagnify the beam and then to make the beam smooth and parallel. The highly scattered electrons from the beam are removed through the condenser aperture. The beam is then passed through a set of coils that is used for scanning the beam. The scanning beam is then passed through the objective lens, which focuses the beam further and then the beam is finally passed through the objective aperture to remove the high angle scattered electrons as shown in Figure 2.2.

When the beam hits the sample, it gives rise to electrons (secondary, backscattered and Auger electrons) and X-rays and is detected by various detectors. All these electrons and X-rays collect different information from the sample underneath. For example the secondary electrons are used for surface topography; backscattered electrons (BSE) have the information about the atomic number and surface topology because they interact with the nucleus of the atom. The atoms with larger nuclei will yield high BSE. Auger electrons are used for surface elemental composition and the X-rays have information about the elemental composition of the bulk of the sample. The SE and BSE are used to image the sample and the X-rays and Auger are normally used for spectroscopy.

Energy dispersive X-ray spectroscopy (EDX)

It is a technique used for the elemental composition of materials. It is based on the principle that when an inner core electron is knocked out by electron beam interaction with the sample, an electron from the higher energy level jumps to the lower level to occupy the inner shell electron space and releases energy, which corresponds to the energy difference between the two energy levels. The characteristics X-rays of the element is also a form of this energy and is shown schematically in Figure 2.3.
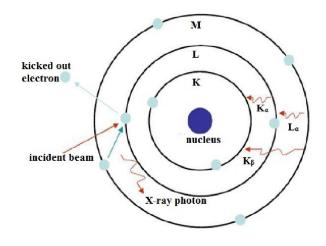

Figure 2.3. Schematic of the EDX phenomenon

Every element emits a specific characteristic X-rays and can be used to identify which specific element is actually present in the specimen. A particular area or spot of a specimen is selected for EDX analysis. The X-rays emitted from the selected area are analyzed through energy dispersive spectrometer for different energies. When an X-ray photon strikes the Lithium-drifted silicon detector it generates photoelectrons. This causes an electron hole pair in the reverse

biased diode and is converted to voltage pulse by a charge sensing amplifier. The pulse is then analyzed through a multichannel analyzer and is sent to the computer. The software then displays the peak after identification and quantifications. The spectrum consists of energy along the x-axis and the counts/intensity along the y-axis, which gives rise to peaks where each peak corresponds to a specific element. Quantitative information about an element in the specimen could also be obtained, which show what weight per cent and what atomic per cent of an individual element does exist in the sample.

Despite the fact that EDX provides a better chemical analysis, however the technique has got some draw backs related to the detection process like, X-ray escape peaks, peak distortion and peak broadening. The escape peak is because of the interaction between the X-ray photon with the detector, which ionizes the Si and results in Auger emission. Some of the Auger electrons recombine in the detector and some of the electrons escape. Therefore the probability of making an electron hole pair is negligibly small. This phenomenon gives rise to escape peak and is equal to the energy of the parent line minus the energy of the Si X-rays. The non-uniformity of the detector near the faces and edges gives rise to recombination and trapping of electrons. This in turn causes the peak distortion. The peak broadening is the result of variation in the number of charge carriers and thermal noise during amplification. This could be overcome only by increasing the collection time.

UV-Vis Spectroscopy

The ultraviolet-visible (UV-Vis) spectrophotometer is an instrument commonly used in the laboratory that analyzes compounds in the ultraviolet (UV) and visible (Vis) regions of the electromagnetic spectrum. The absorption or reflectance in the visible range directly affects the perceived color of the chemicals involved. This technique is complementary to fluorescence spectroscopy. UV/Vis spectroscopy is routinely used in analytical chemistry for the quantitative determination of different analyses, such as transition metal ions, highly conjugated organic compounds, and biological macromolecules. Spectroscopic analysis is commonly carried out in solutions but solids and gases may also be studied. UV/Vis spectroscopy can be used to determine the maximum absorbance as well as wavelength of compounds using Beer-Lambert law,

$$A = \alpha bc$$

Where, A is the absorbance,

α is the molar absorption coefficient
b = path length
c = concentration

Furthermore, the band-gap energy of a compound can be ascertained from this technology by using the equation:

$$E = \frac{hc}{\lambda} \qquad \text{.........................} \quad (3)$$

Where, E is the band gap energy,

h is the Planck's constant

c is the speed of light and

λ is the wavelength of maximum absorption.

Spectrophotometer

A spectrophotometer is employed to measure the amount of light that a sample absorbs. The instrument operates by passing a beam of light through a sample and measuring the intensity of light reaching a detector. When a beam of light consists of steam of photons illuminated a material, photons are absorbed and excitations are created. These excited carriers relax and emit a photon. Then PL spectrum can be collected and analyzed. However, only the energy of photons is equal to or higher than the Band-gap, the absorption can happen in materials. Therefore, we have to choose different excitation source to do the measurements according to different material with different electronic band structure. The PL peak positions reveal transition energies and the PL intensity implicates the relative rates of radiative and non-radiative recombination. Through PL measurement, we can calculate various parameters related to our sample such as (1) Band gap determination (2) Impurity levels and defect detection (3) Recombination mechanisms (4) Material quality

Also the experimental data is used to calculate two quantities: the transmittance (*T*) and the absorbance (*A*).

$$T = \frac{I}{I_0}$$

$$A = -\log_{10} T \qquad (4)$$

....

RESULTS AND DISCUSSION

X-ray Diffraction Analysis

To check the crystallinity and crystal phase of the as-synthesized ZnO nanorods, XRD was performed and results are shown in Fig. 1. All the peaks in the pattern can be indexed to hexagonal phase of bulk ZnO. The diffraction peaks indexed as (100), (002), (101), (102), (110), (103), (200), (112), (201), (004) and (202) planes in XRD pattern are well matched with standard JCPDS card no: 89-7102 indicating the prepared ZnO nanorods. No other impurity peaks were detected in the XRD pattern. Also all diffraction peaks are high intensive and very sharp. Thus high purity hexagonal structured ZnO nanorod could be synthesized by this method.

Optical properties

UV-Vis spectroscopy

The room-temperature optical properties of the ZnO rods were investigated by UV–Vis spectra at room temperature (Fig. 2a). For the UV–Vis measurement, ZnO rods were dispersed in water and measured from these dispersions to detect absorption over the range of 300–600 nm. The obtained UV–Vis absorbance spectrum exhibits a well defined excitonic absorption peak at 376 nm, a corresponding peak for wurtzite

hexagonal phase bulk ZnO. Fig. 2(b) represents tauc plot between $(\alpha h\upsilon)^2$ and E. Using tauc's plot from absorption spectrum the direct bandgap was measured as 3.1 eV.
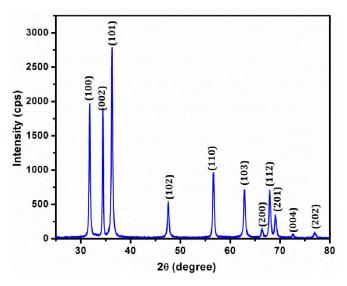

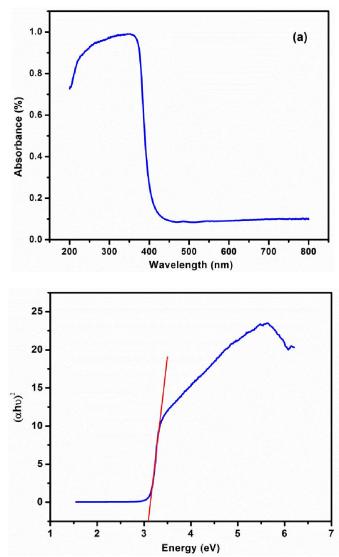**Figure 1. XRD pattern of ZnO nanorods**

Figure 2. (a) UV-Vis absorption spectrum and (b) Tauc plot of ZnO nanorods

Photoluminescence study

Photoluminescence is the one of the important property of ZnO. The room-temperature PL spectrum of ZnO measured using a 325 nm excitation wavelength is shown in Fig. 3.
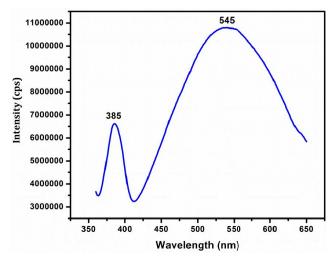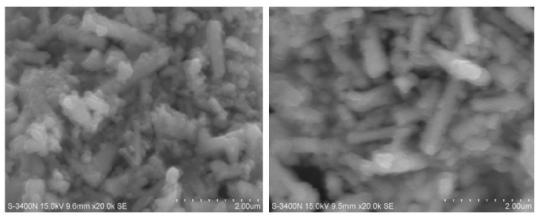

Figure 3. Photoluminescence spectrum of ZnO nanorod

The PL spectrum shows a weak UV emission around 385 nm and a broad yellow emission around 545 nm. In general, the visible emission in ZnO is attributed to different intrinsic defects, such as oxygen vacancies, zinc vacancies, and zinc interstitials. It is observed that ZnO nanorod shows two emission peaks at 385 and 545 nm. UV emission peak centered at 385 nm due to near band edge emission of ZnO. Visible emission peak centered at 545 nm corresponds to oxygen vacancy presents in ZnO nanorod [30].

Surface morphology

Fig. 4 shows SEM image of ZnO nanorods powder resulted from calcinations of zinc hydroxide at 600°C for 4 h. It demonstrates the typical SEM images of micro-sized ZnO nanorods, which has a large quantity of flake shape with a narrow size distribution. It is confirmed from the low-resolution image that the nanorods are synthesized in very large quantity (Fig. 4a). The high-resolution image of the synthesized nanorods reveals that the products have uniform rod shape (Fig. 4b).
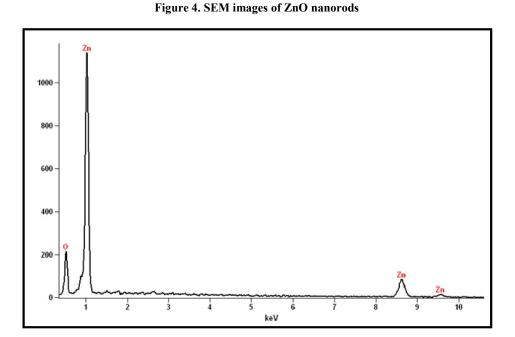

(a)   (b)

Figure 4. SEM images of ZnO nanorods

Figure 5. Energy dispersive spectroscopy of ZnO nanorods

EDAX analysis

Chemical purity and its compositions of the synthesized nanorods were checked by an Energy Dispersive Spectroscopy (EDS) [(Make: HITACHI, Model: S-3400N)]. In EDS spectrum, the oxygen peak corresponding to an energy of about 0.35 k eV and Zn peak corresponding to 1.1, 8.6, 9.5 keV suggests that the as-synthesized ZnO nanorods are composed only of zinc and oxygen elements, which indicates that the product is high-pure ZnO. No other impurities were presented in the sample.

Table 1. Elemental compositions of ZnO nanorods

Element Line	Net Counts	Net Counts Error		Weight %	Atom %	Formula
O K	1125	+/-	67	17.95	47.21	O
Zn K	1518	+/-	86	82.05	52.79	Zn
Zn L	10509	+/-	126	---	---	
Total				100.00	100.00	

Conclusion

ZnO nanorods were successfully synthesized by hydrothermal method. This method is simple, fast and eco-friendly. XRD analysis indicates that single phase hexagonal structure of ZnO. SEM image confirms the rod shape of prepared ZnO sample. EDX spectrum confirms the presence of zinc and oxygen only. The optical bandgap of ZnO nanorod was found to be 3.1 eV. The ZnO nanorods were found to show strong band edge emission with very weak or no deep-level emission, as shown by photoluminescence measurements. Moreover, the rod-like ZnO had a very strong UV emission at about 385 nm, which might be very interesting for further application to microscale optoelectronic devices due to their excellent UV emission properties.

REFERENCES

Ahsanulhaq Qurashi, Jahangir Ahmad Rather, Karolien De Wael, Belabbes Merzougui, 2013. Naour Tabet and Mohammed Faiz, *Analyst*, Vol. 138, 4764–4768.

Baruah, S and Dutta, J. 2009. *Science and Technology of Advanced Materials*, Vol. 10 (1).

Chen, Z., Z. Shan, S. Li, C.B. Liang, and S.X. Mao, 2004. *Journal of Crystal Growth*, Vol. 265, 482–486.

Djurisic, A.B. Ng, A.M.C. Chen, X.Y. 2010. Progress in Quantum Electronics, Vol. 34, 191–259.

Fanfei Bai, T., Ping He, Zhijie Jia, Xintang Huang, Yun He, 2005. *Materials letters*, Vol. 59, 1687-1690.

Fanfei Bai, T., Ping He, Zhijie Jia, Xintang Huang, Yun He, 2005. *Materials letters*, Vol. 59, 1687-1690.

Ghule, L. A. Shirke, B. S. Sapnar, K. B. Dhole, S. D. Hankare, P. P. Garadkar, K. M. 2011. *Journal of Materials Science: Materials in Electronics*, Vol. 22, 1120-1123.

http://www.chemistry.ohio-state.edu/~woodward/ch754/struct/ZnO.htm

Juan Xie, Ping Li, Yanji Wang,YuWe, 2009. *Journal of Physics and Chemistry of Solids*, Vol. 70 112–116.

Law, M., Greene, L. E., Jhonson, J. C., Saykally, R., Yang, P., 2005. *Nat. Mater.,* Vol. 4, 455–459.

Michelle, J.S. Spencer, 2012. Progress in Materials Science, Vol. 57, 437–486.

Polsongkram, D. Chamninok, P. Pukird, S. Chow, L. Lupan, O. Chai, G. Khallaf, H. Park, S. Schulte, A.2008. *Physica B*, Vol. 403, 3713-3717.

Saito, N. Haneda, H. 2011. *Sci. Technol. Adv. Mater.,* Vol. 12, 064707.

Saravanan, R. Kalavathy Santhi, N. Sivakumar, V. Narayanan, A. Stephen, 2012. *Materials Characterization*, Vol. 67, 10-16.

Sarika, D. Shinde, G. E. Patil, D. D. Kajale, D. V. Ahire, V. B. Gaikwad and G. H. 2012. Jain, *International journal of smart sensing and intelligent system*, Vol. 5, 57-70.

Sekar, A., S. H. Kim, A. Umar and Y. B. Hahn, 2005. *Journal of Crystal Growth*, Vol. 277, 471–478.

Seung-Ho Jung, Seung-Ho Jung,Eugene Oh, Kun-Hong Lee, Yosep Yang, Chan Gyung Park, Wanjun Park and Soo-Hwan Jeong, 2008. *Crystal growth and design*, Vol. 8, 265-269.

Subramanyam, T. K. Srinivasulu Naidu, B. Uthanna, S. 2000. *Cryst. Res. Technol.* Vol. 35 (10), 1194-1202

Tam, K.H. Djurisic, A.B. Chan, C.M.N. Xi, Y.Y. Tse, C.W. Leung, Y.H. Chan, W.K. Leung, F.C.C. Au, D.W.T. 2008. *Thin solid films*, Vol. 516, 6167-6174.

Tian, Y., Li, J., Xiong, H., Dai, J., 2011. *Applied Surface Science,* Vol. 22(258), 8431-8438.

Wang, H., Jiang, H., Zhang, H., Zhou, Y., Wu, C., Zhao, J., Wu, C., Ba, L., Wang, X., 2011. *J Nanosci Nanotechnology,* Vol. 11(2):1117-22

Xiaobin Xu, Min Wu, Michael Asoro, P. J. Ferreira, and D. L. Fan, 2012. *Crystal Growth Design*, Vol. 12 (10), 4829–4833.

Xudong Wang, Jinhui Song and Zhong Lin Wang, 2007. *Journal of Material Chemistry*, Vol. 17, 711–720.

Zafar Hussain Ibupoto, Kimleang Khun, Martin Eriksson, Mohammad AlSalhi, Muhammad Atif, Anees Ansari and Magnus Willander, 2013. *Materials*, Vol. 6, 3584-3597.

Zhang, J., Y. Yang, B. Xu, F. Jiang, and J. Li. 2005. *Journal of Crystal Growth*, Vol. 280, pp.509–515.

Zhiyong Fan and Jia G. Lu, 2005. *Journal of Nanoscience and Nanotechnology*. Vol. 5, pp. 1561-1573.

Zhong Lin Wang, 2004. *Journal of Physics: Condensed Matter*, Vol. 16, R829-R858.

Zhong Lin Wang, 2014. *Materials Today*, 26-33.

****